

Collision spectroscopy of the He⁺-CO, He⁺-NO, He-CO, and He-NO systems

D. Doweck, D. Dhucq, and M. Barat

*Laboratoire des Collisions Atomiques et Moléculaires, Bâtiment 351, Université de Paris—Sud,
F-91405 Orsay Cedex, France*

(Received 21 September 1982)

We present a comprehensive investigation of the He⁺-CO, He⁺-NO, He-CO, and He-NO collisions in the $0.5 < E_{\text{lab}} < 3$ -keV energy range. The comparison of ionic and neutral systems allows a determination of the excitation mechanisms that are common or specific to each case. In the course of this study new states of the CO⁺ and NO⁺ molecular ions were discovered. The previously proposed excitation mechanisms—(i) direct Demkov-type transitions populating the exothermic charge-exchange channels, (ii) molecular-orbital (MO) promotion giving rise to MO crossings and subsequent electron transitions, and (iii) two-electron transitions leading to direct-excitation and charge-exchange processes in the ionic systems—are also found to apply to the present case, thus confirming their generality.

I. INTRODUCTION

This paper is the third in a series investigating the direct and charge-exchange processes in atom-diatom collisions. The qualitative interpretation of the excitation mechanisms in He⁺-N₂ and -O₂ collisions¹ was based on the extrapolation of the knowledge accumulated previously from ion-atom collisions. The comparison of the simple neutral He-H₂ and ionic He⁺-H₂ systems² established that three types of mechanisms govern inelastic processes in such collisions in the medium-energy range ($0.5 < E < 3$ keV). Common to both neutral and ionic systems, crossings between molecular-orbital (MO) surfaces occur at which electron transitions are favored. This regime is generally found for hard collisions ($\tau = E\theta > 1.5$ keV deg) where the relevant crossings arise because of the molecular-orbital promotion (diabatic-I mechanism³ DI). Specific to the ionic He⁺-BC systems, the initial vacancy in the He 1s orbital becomes an inner vacancy in the quasimolecule; this implies that the incident channel is a core excited configuration of the quasimolecule, which crosses an infinite series of Rydberg states with filled cores. This mechanism, referred to as the diabatic-II (DII) mechanism,³ is efficient for soft collisions, i.e., $\tau < 1$ keV deg. Finally, in He⁺-BC collisions a *direct* transition^{1,2} populates the near-resonant channels and, in particular, the exothermic charge-exchange channels.

In this paper we extend our previous work^{1,2} to collisions of the He and He⁺ projectiles with CO and NO asymmetric targets. Our objectives were to study the following:

- (i) heteronuclear targets;
- (ii) the role of the He 1s vacancy in complex systems by the comparison of ionic and corresponding neutral collision systems;
- (iii) whether the dominant excitation of endothermic versus exothermic charge exchange channels, found for the He⁺-N₂, -O₂, and -H₂ systems, is a common feature of all the He⁺-target collisions; and
- (iv) the ability of collision spectroscopy to explore highly excited states of molecular ions.

Most material available in the literature on the He⁽⁺⁾-CO and -NO collisions is devoted to the charge-exchange process. In the medium-energy range large total electron-capture cross sections have been measured by several authors^{4,5}: $\sigma_{\text{EC}} \cong 0.7 \times 10^{-15}$ cm² for the He⁺-CO collisions and $\sigma_{\text{EC}} \cong 1 \times 10^{-15}$ cm² for the He⁺-NO collisions. This suggests that a near-resonant electron-capture process occurs in the He⁺-CO and -NO collisions. These authors were not able to identify the CO⁺⁺ (NO⁺⁺) excited states involved in this electron-capture process. However, from the measurement of the relative abundance of the C⁺, O⁺, and CO⁺ (N⁺, O⁺, and NO⁺) products^{6,7} it was inferred that the molecular ions were formed dominantly in dissociative or predissociative states.

The energy-loss measurements presented in Sec. III B for He⁺-CO and Sec. IV B for He⁺-NO allow us to locate the relevant molecular ion states in the Franck-Condon (FC) region. These energy-loss measurements are carried out as a function of the scattering angle θ and thus provide a determination of the relative probabilities of all direct excitation and charge exchange inelastic processes. Similar measurements are reported for the related He-CO and -NO systems (Secs. III A and IV A) in order to firmly establish the basic similarities and differences of the excitation mechanisms involved in ionic and neutral He⁽⁺⁾-BC collisions.

II. EXPERIMENTAL TECHNIQUE

Identification of the various direct excitation and charge-exchange processes is achieved by measuring the characteristic kinetic energy losses undergone by the scattered He or He⁺ projectile. The experimental setups have been described elsewhere.^{1,8} Briefly, a focused He⁺ beam is produced from a discharge ion source (and passed through a charge-exchange cell filled with He if a fast He neutral beam is needed) and directed into the collision chamber. The neutral particles scattered at a given angle are energy analyzed using a time-of-flight (TOF) technique (energy resolution $\Delta E \cong 0.3$ eV at $E = 1$ keV). The scattered ions can be energy analyzed using the TOF method or pass through a 127° electrostatic analyzer.

From the relative areas under the peaks of the energy-loss spectra (ELS) the relative probability for a given process is determined. The relative calibration of direct excitation and charge-exchange processes is required to determine these probabilities for the He⁺-CO, -NO ionic systems. This is achieved by measuring the total number of scattered particles ($N + I$) with the electrostatic analyzer voltage off and the number of neutrals N with the analyzer voltage on. Experimental difficulties arise for the determination of this $N/(N + I)$ ratio at a small scattering angle ($\theta < 1^\circ$) due to the angular spread of the incident beam. This deficiency of the experimental technique hinders accurate relative probability measurements at small reduced angle τ . In some cases, the reduced differential cross sections $\rho(\tau) \approx \sigma(\theta)\theta \sin\theta$ have also been determined.

III. EXPERIMENTAL RESULTS: He⁽⁺⁾-CO COLLISIONS

A. He-CO neutral system

1. Energy-loss spectra

Typical energy-loss spectra (ELS) are displayed in Fig. 1. Beside elastic scattering (X), four inelastic structures labeled α , β_1 , β_2 , and β_3 reveal the excitation of singly and doubly excited states of the CO target. It is noteworthy that the first electronic state of CO ($a^3\Pi$, $Q = 6$ eV) is not observed; this is in agreement with the Wigner spin conservation rule which will therefore be assumed to hold. The structures can be identified as follows [see Table I(a)].

α , $7 < Q < 11$ eV. Using the CO potential-energy curves⁹ in the FC region one can identify the double structure α as the excitation of the $A^1\Pi$ ($Q \cong 8.4$ eV) and the $D^1\Delta$ (or $I^1\Sigma^-$) ($Q \cong 9.8$ eV) valence states.

β_1 , $11 < Q < 14$ eV. This peak corresponds to the weak excitation of the ($5\sigma \rightarrow n1\lambda$) Rydberg series converging to the $\text{CO}^+(X^2\Sigma^+)$ limit.¹⁰

β_2 , $14 < Q < 18.5$ eV. Structure β_2 is attributed to the excitation of the Rydberg states converging to the $\text{CO}^{++}(A^2\Pi)$ limit, characterized by the excitation of a 1π electron. In particular, the energy loss which corresponds to the maximum of the β_2 peak can be associated with the $(1\pi)^1\Sigma^+ \rightarrow (n\delta)^1\Pi$ Rydberg series.¹⁰

β_3 , $20 < Q < 25$ eV. The β_3 broad peak having its maximum around $Q_{\text{max}} = 22$ eV is ascribed to the excitation of a series of CO^{**} autoionizing states involving the excitation of two core electrons; this series converges to the $\text{CO}^{++}(D^2\Pi)$ ($Q \cong 22.7$ eV) and $\text{CO}^{++}(C^2\Sigma^+)$ ($Q \cong 24$ eV) limits (Ref. 11). The absence of significant structure around 20 eV, where the $\text{CO}^{++}(B^2\Sigma^+)$ ionic state lies, shows that the excitation of the electrons belonging to the 4σ molecular orbital does not occur. This β_3 structure might also be ascribed to direct excitation of singlet states of He ($20.1 < Q < 24.6$ eV), although in such a case one would expect to observe the He* structure owing to the energy resolution in the ELS.

At a large reduced angle ($\tau \cong 4$ keV deg) a broad tail covers the range between 25 and 40 eV where the CO^{2+} limit lies.

Spectroscopic analysis of optical emissions resulting from He-CO collision¹² performed in this energy range

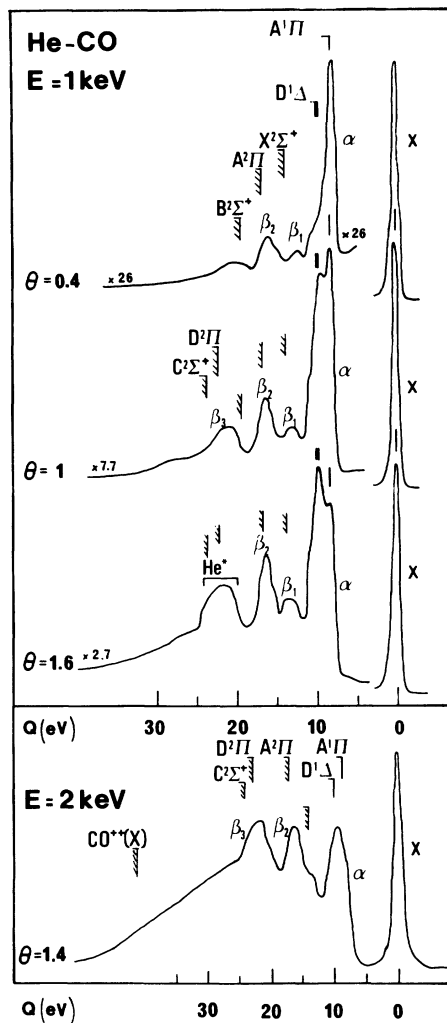
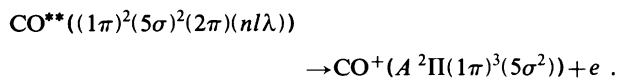


FIG. 1. ELS of scattered He from He-CO collision as a function of scattering angle θ . Peaks labeled $X, \alpha, \beta_1, \beta_2, \beta_3$, refer to elastic scattering (X) and excitation of electronic states of CO. [See text and Table I(a) for the identification of the molecular states.]

shows that a substantial population of the $\text{CO}^+(A^2\Pi)$ state is observed; this is probably related to the strong excitation of autoionizing CO^{**} states above the $\text{CO}^+(A^2\Pi)$ limit, which may decay as



[The optical results also display weak lines from triplet He states: If, as stated above, the spin conservation rule is valid, these triplet He lines should not be produced by direct excitation of the projectile, but more probably result from the He(2^3S) state which is a component of the incident beam in those experiments.¹²]

2. Relative probabilities of collision processes

The excitation probabilities for elastic scattering and inelastic processes as a function of the reduced angle τ are

TABLE I. Identification of inelastic processes in (a) He-CO and (b) He⁺-CO collisions.

Observed process	CO excitation	Electronic configuration				
		4σ	1π	5σ	2π	nλ
(a)						
<i>X</i>	<i>X</i> 1Σ ⁺	2	4	2		
α ₁	<i>A</i> 1Π	2	4	1	1	
α ₂	<i>D</i> 1Δ, <i>I</i> 1Σ ⁻	2	3	2	1	
β ₁	CO ⁺ (<i>X</i>) + e _{Ryd}	2	4	1	0	1
β ₂	CO ⁺ (<i>A</i> 2Π) + e _{Ryd}	2	3	2	0	1
β ₃	CO ⁺ (<i>D</i> 2Π) + e _{Ryd}	2	2	2	1	1
	CO ⁺ (<i>C</i> 2Σ ⁺) + e _{Ryd}	2	3	1	1	1
Direct	CO excitation					
(b)						
<i>X</i>	<i>X</i> 1Σ ⁺	2	4	2		
α' ₀	<i>a</i> 3Π	2	4	1	1	
α'	<i>A</i> 1Π	2	4	1	1	
	<i>D</i> 1Δ, <i>I</i> 1Σ ⁻	2	3	2	1	
β' ₁	CO ⁺ (<i>X</i>) + e _{Ryd}	2	4	1	0	1
β' ₂	CO ⁺ (<i>A</i> 2Π) + e _{Ryd}	2	3	2	0	1
β' ₃	CO ⁺ (<i>D</i> 2Π) + e _{Ryd}	2	2	2	1	1
	CO ⁺ (<i>C</i> 2Σ ⁺) + e _{Ryd}	2	3	1	1	1
Exchange	CO ⁺ excitation					
γ	<i>C</i> 2Σ ⁺	2	3	1	1	
δ ₂	<i>B</i> 2Σ ⁺	1	4	2		
δ ₂	<i>A</i> 2Π	2	3	2		
δ ₃	<i>X</i> 2Σ ⁺	2	4	1		
ε, η, ψ	<i>F</i> 2Σ ⁺ , 2Σ ⁺	1	3	2	1	

shown in Figs. 2(a) and 3(a) for $E = 0.5$ and 1 keV. They are defined by

$$P_i(\tau) = \frac{I_i(\tau)}{I_{el}(\tau) + \sum_i I_i(\tau)}, \quad (1)$$

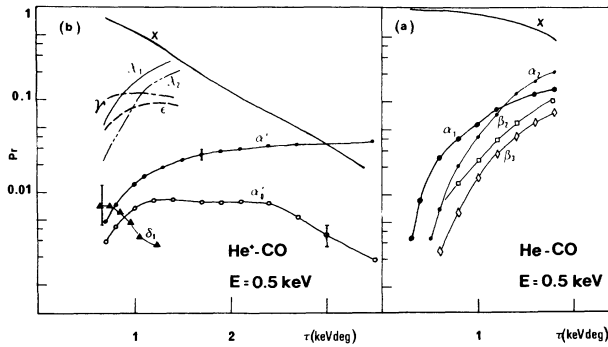


FIG. 2. (a) Relative probabilities P_i of electronic excitation of CO by He impact at $E = 0.5$ keV, as a function of the reduced angle τ . X refers to elastic scattering and $\alpha_1, \alpha_2, \beta_1, \beta_2, \beta_3$ refer to the various electronic excited states of CO. Identification is given in the text and in Table I(a). (b) Relative probabilities P_i for direct excitation (α'_0, α') and electron capture ($\gamma, \epsilon, \delta, \chi_1, \chi_2$) processes in He⁺-CO collisions at $E = 0.5$ keV, as a function of the reduced angle τ . In order to clarify the presentation of the data, several charge-exchange channels which display similar τ and E dependence have been summed for the following energy-loss slices: χ_1 , $5 < Q < 12$ eV; χ_2 , $12 < Q < 17$ eV; and χ_3 , $Q > 17$ eV. δ stands for the sum of all exothermic channels.

where $I_i(\tau)$ stands for the area under the peak i and I_{el} stands for the area under the elastic peak. The relative probabilities increase with increasing τ for all inelastic processes. Those which correspond to the excitation of valence states (α) reach a maximum around 1 keV deg and 1.5 keV, whereas those associated with doubly excited states keep on increasing in the observed τ range, reaching a plateau around $\tau = 4$ keV deg at $E = 2$ keV.

B. He⁺-CO collisions

Now we turn to the data for the ionic He⁺-CO system. We present them in the following three subsections.

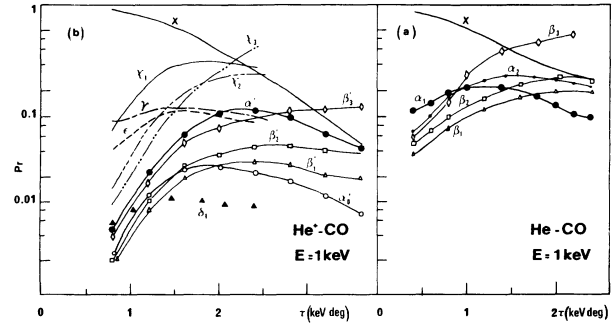


FIG. 3. (a) Relative probabilities P_i of electronic excitation of CO by He impact at $E = 1$ keV, as a function of τ . X refers to elastic scattering and $\alpha_1, \alpha_2, \beta_1, \beta_2, \beta_3$ refer to the various electronic states of CO. [See text and Table I(a).] (b) Relative probabilities P_i for direct excitation ($\alpha'_0, \alpha', \beta'_1, \beta'_2, \beta'_3$) and electron capture ($\gamma, \epsilon, \delta, \chi_1, \chi_2, \chi_3$) processes in He⁺-CO collision at $E = 1$ keV. χ_1, χ_2 , and χ_3 are defined in Fig. 2(b).

1. Energy-loss spectra: direct excitation

The energy analysis of the scattered He⁺ projectiles enables the identification of the CO excited states. Figure 4 shows that the CO (*a*³Π) state ($\alpha'_0 Q \cong 6$ eV) now appears among the other singly excited states of CO(α'). This is consistent with the fact that no spin selection rule prevents this state from being excited. At low reduced angle excitation of the Rydberg series (β'_1) converging to the CO⁺(*X*) ground state dominates the $Q > 11$ -eV energy-loss range, whereas for larger τ values ($\tau \geq 2$ keV deg) the two β'_2 ($14 < Q < 18.5$) and β'_3 ($20 < Q < 25$ eV) structures involving CO⁺(*A*²Π) and CO⁺(*D*²Π) excited ionized limits become increasingly dominant. The behavior of both β'_1 and β'_2 is therefore similar to what was observed for the He-CO neutral system [see Table I(b)].

2. Energy-loss spectra: electron-capture processes

The energy analysis of the scattered neutralized He projectiles enables the identification of the CO⁺ excited states, with or without simultaneous He excitation. At low energy $E < 500$ eV and small scattering angle $\theta < 0.5^\circ$ a single peak γ is observed which corresponds to a near-

resonant charge-exchange process (Fig. 5). Three electronic states of CO⁺ discussed in the literature may contribute to this process; namely, the *C*²Σ⁺, *D*²Π, and ²Δ states.^{11,13} The measured full width at half maximum (FWHM) of the γ peak ($\delta E \cong 1.5$ eV) favors the identification of the *C*²Σ⁺ state since the *D*²Π and ²Δ curves exhibit a more repulsive shape than the *C*²Σ⁺ curve,¹³ which would give rise to a broader FC distribution ($\delta E \cong 3$ and 4 eV, respectively).

When the reduced angle increases, other charge-exchange channels show up: The salient feature of the spectra is the strongly unbalanced excitation of exothermic and endothermic channels, similar to our earlier results for the He⁺-N₂, -O₂, and -H₂ collisions.^{1,2} In both cases the excitation of endothermic charge-exchange channels dominates the excitation of the exothermic ones.

a. Exothermic channels: $Q < 0$. Apart from the *C*²Σ⁺ and *D*²Π CO⁺ states, which lie close to resonance, the ELS displayed in Fig. 5 show that electron-capture processes populate three exothermic channels which are unambiguously identified (in eV):

$$\text{He}(1s^2) + \begin{cases} \text{CO}^+(B^2\Sigma^+) (\delta_1), & \text{with } Q \cong -4.9 \\ \text{CO}^+(A^2\Pi) (\delta_2), & \text{with } Q \cong -7.5 \\ \text{CO}^+(X) (\delta_3), & \text{with } Q \cong -10.6. \end{cases}$$

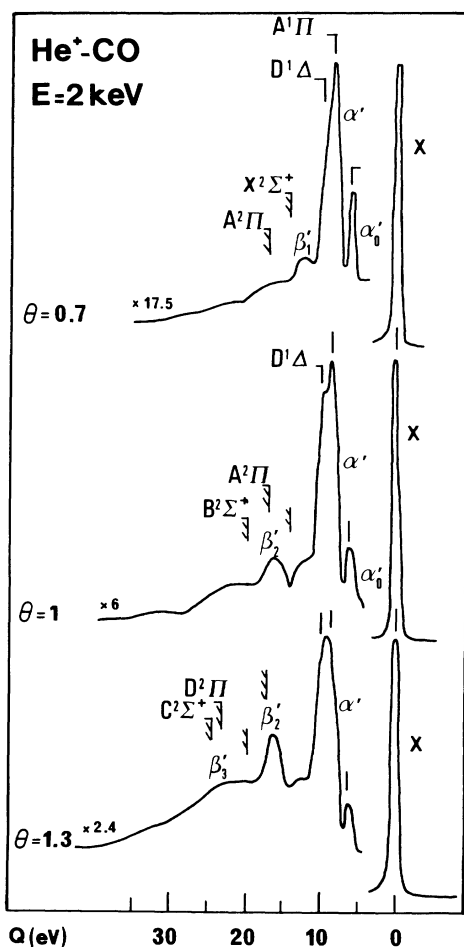


FIG. 4. ELS of scattered He⁺ from He⁺-CO collision as a function of scattering angle θ . [See text and Table I(b) for the identification of the molecular states.]

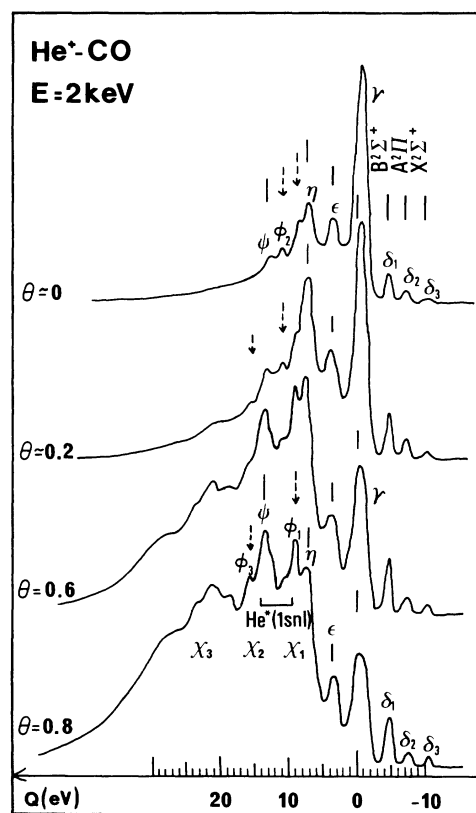


FIG. 5. ELS of scattered neutral He from He⁺-CO collision as a function of scattering angle. [See text and Table I(b) for the identification of the molecular states.] Dashed arrows correspond to new states of CO⁺, the identification of which is discussed in the text.

The relative intensity of these channels remains small.

b. Endothermic channels: $Q > 0$. A number of endothermic channels are excited and their relative intensity strongly increases with increasing E and τ . Identification of these structures requires a detailed knowledge of the CO^+ excited states which lie at least 25 eV above the $\text{CO}(X)$ state in the FC region. The available experimental data in the 25–40-eV excitation energy region consist of absorption spectra of CO obtained by electron synchrotron radiation,¹⁴ weak excitation of “forbidden” bands in photoelectron spectra¹⁵ and detection of fragment ions produced by dissociative ionization^{13,16} of CO. The accurate identification of the CO^{++} states which could be deduced

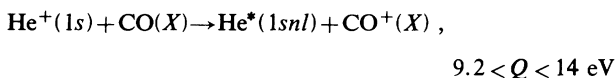
$$\text{He}(1s^2) + \begin{cases} \text{CO}^+(F^2\Sigma^+) (\epsilon), & \text{with } Q \cong 3.2 \text{ and } \Delta E \cong 27.8 \\ \text{CO}^+(^2\Sigma^+) (\eta), & \text{with } Q \cong 7.2 \text{ and } \Delta E \cong 31.8 \\ \text{CO}^+((3\sigma)^{-1}{}^2\Sigma^+) (\psi), & \text{with } Q \cong 13 \text{ and } \Delta E \cong 37.6 . \end{cases}$$

[ΔE is the energy position of the considered CO^{++} state above the $\text{CO}(^1\Sigma^+)$ ground state in the FC region.] It is noteworthy that these energy-loss measurements constitute the first experimental data showing strong resolved excitation of the $\text{CO}^+(F^2\Sigma^+)$ ($\Delta E \cong 28$ eV) and $\text{CO}^+(^2\Sigma^+)$ ($\Delta E \cong 31.8$ eV) ionic states.

Three additional peaks located at $Q \cong 8.6$ eV (ϕ_1), $Q \cong 10.5$ eV (ϕ_2), and $Q \cong 15.5$ -eV (ϕ_3) (± 0.2 -eV) energy losses are observed. As a reasonable guess, these peaks can be attributed to the excitation of CO^{++} states. Accordingly, their energy positions in the FC region are $\Delta E \cong 33.2$, 35, and 40.1 eV (± 0.2 eV), respectively. Except for the $\text{CO}^+(3\sigma)^{-1}{}^2\Sigma^+$ (ψ) state, there are no other CO^+ states which differ by a single electron from the CO ground state in this energy range. Consequently, the CO^{++} states associated with peaks ϕ_i most probably arise from electronic configurations which differ by two electrons from the CO ground state as do the $\text{CO}^+(F^2\Sigma^+)$ (ϵ) and $\text{CO}^+(^2\Sigma^+)$ (η) states. In particular, these electronic configurations should be obtained by rearranging two electrons from the 4σ , 1π , and/or 5σ outermost CO molecular orbitals: such states can be labeled

$$\text{CO}^{++} [(4\sigma)^2(1\pi)^4(5\sigma)^2]n\lambda .$$

Peaks ψ and ϕ_2 can alternatively be ascribed to the electron-capture process into excited states of He:



which partially overlap the discussed energy-loss range. Observation of He lines in optical studies of He^+ -CO collisions¹⁷ could be an indication of the occurrence of this process. However, the simultaneous excitation of both He and CO^+ can also account for the optical results. The latter process certainly contributes to the broad structures ($Q \cong 17$ –40 eV) superimposed on the tail corresponding to the transfer ionization,



$$Q \cong 16 \text{ eV} .$$

from these data remains limited. Furthermore, the theoretical predictions of such states are even more scarce, although configuration-interaction CNDO/INDO calculations have been performed which determine the vertical ionization potentials of few CO^+ states in the 25–38-eV energy range.¹¹

When possible, the identification of the charge-exchange processes was based on the above data. Otherwise, previously unreported CO^{++} states are proposed to explain our experimental results. In this context, the following identification can be made [Table I(b)]; the units are in eV and are further referred to in Refs. 11 and 13 for the first identification, while the latter are from Ref. 11:

3. Relative probabilities of the collision processes

The relative probabilities for direct and exchange processes defined by formula (1) are displayed in Figs. 2(b) and 3(b). Figure 6 shows the corresponding reduced differential cross sections (DCS) as a function of the reduced angle τ at $E = 0.5$ keV.

The salient feature of these data is the dominance of electron-capture processes for $\tau > 1$ keV deg². The near-resonant charge-exchange process (γ) is found to be dominant for the small τ values ($\tau \leq 0.5$ keV deg) and to slowly decrease with increasing τ at a given energy. The ϵ charge-exchange channel behaves very similarly whereas

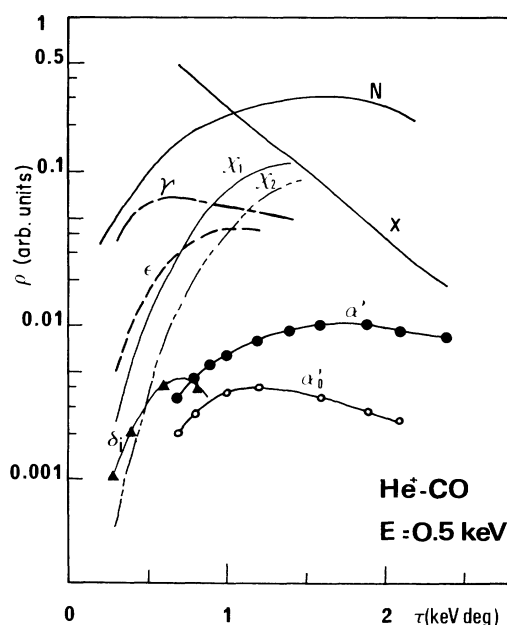


FIG. 6. Reduced differential cross sections for the He^+ -CO collision at $E = 0.5$ keV, as a function of τ . Curves labeled X and N refer to the elastic scattering and the sum of all charge-exchange processes, respectively. $\gamma, \epsilon, \delta, \chi_1, \chi_2, \alpha_0', \alpha_1'$ refer to the various inelastic channels defined in the text and in Table I(b).

the other endothermic channels (χ_1, χ_2, χ_3) increase strongly with increasing τ and become dominant for $\tau > 0.8$ keV deg at $E = 1$ keV.

The exothermic charge-exchange process remains very weak, consistent with optical data¹⁷ which show that the measured absolute cross sections for the CO⁺(A→X) ($\sigma = 3 \times 10^{-17}$ cm² at $E = 1$ keV) and the CO⁺(B→X) ($\sigma \cong 1.7 \times 10^{-17}$ cm² at $E = 1$ keV) transitions are very weak compared with the total charge-exchange cross section (10^{-15} cm²). However, the relative importance of the CO⁺(A²Π) and CO⁺(B²Σ⁺) production ascribed to the electron-capture process ($\sigma_{A^2\Pi} > \sigma_{B^2\Sigma^+}$) in the optical investigation is in disagreement with the present data which show a preferential excitation of the (He 1s² + CO⁺ B) exothermic channel. This apparent disagreement may be due to other processes such as direct ionization, simultaneous excitation of He and CO⁺, etc., which are included in the optical measurement but not in our data.

Figure 7 displays the energy dependence of the relative probabilities of excitation of some charge-exchange channels. The importance of channels γ , ϵ , and χ_1 decreases with increasing energy, contrasting with the increasing importance of the doubly excited and transfer ionization channels χ_3 .

The relative probabilities of the direct excitation of CO valence states (α') exhibit a flat maximum around $\tau = 2$ keV deg whereas those associated with excited Rydberg series ($\beta_1, \beta_2, \beta_3$) slowly increase with τ . The relative importance of these direct excitation channels slowly increases with increasing energy.

Inspection of the present data shows that in the medium-energy range the near-resonant and endothermic charge-exchange processes γ and χ_i respectively provide the major contribution to the production of CO⁺ excited states. These CO⁺ states are located in the 24.6–60-eV energy range above the CO(X) ground state in the FC region. The connection of these data with the measurements of the relative abundance of C⁺, O⁺, and CO⁺ ions in the He⁺-CO collision⁶: $I_{C^+} \gg I_{O^+} \gg I_{CO^+}$ shows that these

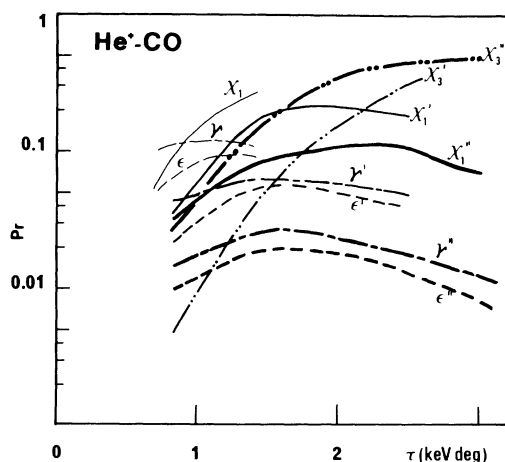


FIG. 7. Energy dependence of the relative probabilities associated with some typical charge-exchange channels defined in the text and in Table I(b). Light curves (γ, ϵ, χ_1), intermediate curves ($\gamma', \epsilon', \chi_1', \chi_3'$), and thick curves ($\gamma'', \epsilon'', \chi_1'', \chi_3''$) correspond to $E = 0.5, 1,$ and 2 keV, respectively.

CO⁺ excited states are mainly dissociative or predissociative states. Besides, the comparison of the present results with the data for ionization and fragmentation of CO photon^{15(a)} and keV electron impact^{16(a)} ($4.4 < I_{C^+}/I_{CO^+} < 25.5\%$ and $0.05 < I_{O^+}/I_{CO^+} < 24\%$) indicates that the He⁺ ion impact provides complementary information on the excited states of CO⁺ in the 20–60-eV energy range.

IV. EXPERIMENTAL RESULTS: He⁽⁺⁾-NO COLLISIONS

Now we shift to the He and He⁺-NO collisions. As before the idea is to compare the neutral and ionic systems.

A. He-NO collisions

1. Energy-loss spectra

Figure 8 shows that one- and two-electron excited states of the NO target are produced by the collision. We have excluded from consideration the quartet NO states which should not be excited according to the spin conservation rule. The observed structures are identified as follows [see Table II(a)].

α , $6 \leq Q \leq 10$ eV. Using the NO potential-energy curves¹⁸ in the FC region, we ascribe this structure to the

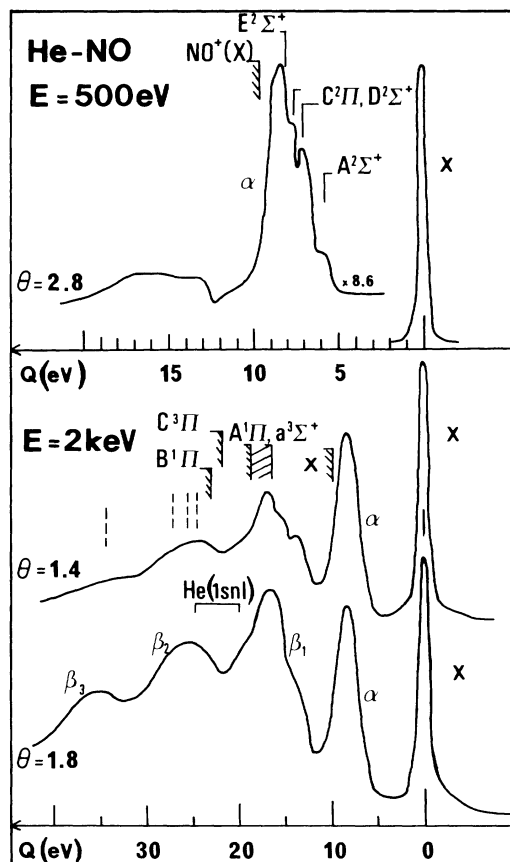


FIG. 8. ELS of scattered He from He-NO collision as a function of scattering angle θ . Peaks labeled $\chi, \alpha, \beta_1, \beta_2, \beta_3$, refer to elastic scattering (X) and excitation of electronic states of NO. [See text and Table II(a) for the identification of the molecular states.]

TABLE II. Identification of inelastic processes in (a) He-NO and (b) He⁺-NO collisions.

Observed process	NO excitation	Electronic configuration				
		4σ	5σ	1π	2π	n 1λ
(a)						
<i>X</i>	<i>X</i> ² Π	2	2	4	1	
<i>α</i>	<i>C</i> ² Π, <i>D</i> ² Σ ⁺	2	2	4	0	1
	<i>B</i> ² Π	2	2	3	2	
<i>β</i> ₁	NO ⁺ (<i>a</i> ³ Σ ⁺) + <i>e</i> _{Ryd}	2	2	3	1	1
	NO ⁺ (<i>A</i> ¹ Π or <i>b</i> ³ Π) + <i>e</i> _{Ryd}	2	1	4	1	1
<i>β</i> ₂ , <i>β</i> ₃		2	2	2	2	1
		2	1	3	2	1
(b)						
<i>X</i>	<i>X</i> ² Π	2	2	4	1	
<i>α</i> ' ₀	<i>a</i> ⁴ Π	2	2	3	2	
	<i>A</i> ² Σ ⁺	2	2	4	1	3 <i>sσ</i>
<i>α</i> '	<i>C</i> ² Π, <i>D</i> ² Σ ⁺	2	2	4	0	1
	<i>B</i> ² Π	2	2	3	2	
<i>β</i> ' ₁	NO ⁺ (<i>a</i> ³ Σ ⁺) + <i>e</i> _{Ryd}	2	2	3	1	1
	NO ⁺ (<i>A</i> ¹ Π or <i>b</i> ³ Π) + <i>e</i> _{Ryd}	2	1	4	1	1
<i>β</i> ' ₂ , <i>β</i> ' ₃		2	2	2	2	1
		2	1	3	2	1
Exchange						
	NO ⁺ excitation					
<i>δ</i> ₁	<i>B</i> ¹ Π, <i>B</i> ' ¹ Σ ⁺	1	2	4	1	
<i>δ</i> ₂	<i>C</i> ³ Π	1	2	4	1	
<i>δ</i> ₃	<i>A</i> ¹ Π	2	1	4	1	
<i>δ</i> ₄	<i>b</i> ³ Π	2	1	4	1	
	<i>a</i> ³ Σ ⁺	2	2	3	1	
<i>δ</i> ₅	<i>X</i>	2	2	4	0	

excitation of the *C*²Π and/or *D*²Σ⁺ ($Q \cong 6.8$ eV), *E*²Σ⁺, *F*²Δ, ... ($Q \cong 8$ eV) Rydberg states of NO. It is noteworthy that the *A*²Σ⁺ first state of this series is very weakly excited. The step observed at $Q = 7.5$ eV is probably due to the excitation of the *B*²Π valence state.

*β*₁, $12 < Q < 20$ eV. This broad structure which displays three maxima ($Q \cong 13, 15.5, \text{ and } 17$ eV) corresponding to the excitation of core-excited Rydberg¹⁹ series converging to the various (*a*³Σ⁺, *b*³Π, . . . , *A*¹Π) NO⁺ limits.²⁰

*β*₂, $22 \leq Q \leq 32$ eV; *β*₃, $32 \leq Q \leq 40$ eV. Appropriate data to identify these structures are not present in the literature. We suggest that the *β*₂ and *β*₃ peaks correspond to series of doubly excited states of NO, converging to the core excited NO⁺ limits ($\Delta E \cong 24.6, 25.1, 26.2, \text{ and } 34.5$ eV in the FC region) discussed in Sec. IV B 2.

The absence of significant structure around 22–23 eV where the NO⁺⁺ (*C*³Π, *B*¹Π) states lie suggests that the 4σ core electrons are not excited during the He-NO collision, similar to the He-CO case.

No structure is observed in the 20–24.6-eV energy-loss range indicating the absence of He excitation (cf. He-CO).

2. Relative probabilities

The relative probabilities of elastic scattering (*X*) excitation of the low-lying excited NO states (*α*) ($Q < 11$ eV) and excitation of the various Rydberg series (*β*₁, *β*₂, *β*₃) as functions of the reduced angle τ at $E = 0.5$ and 1 keV are displayed in Figs. 9(a) and 10(a), respectively.

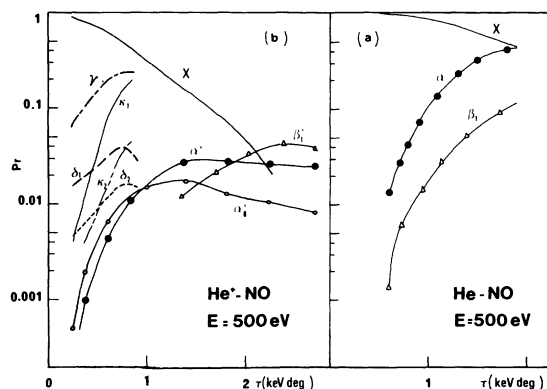


FIG. 9. (a) Relative probabilities P_r of electronic excitation of NO by He impact at $E = 0.5$ keV, as a function of τ . *X* refers to elastic scattering and *α*, *β*₁, refer to the electronic excited states of NO. Identification is given in the text and in Table II(a). (b) Relative probabilities P_r for direct excitation (*α*'₀, *α*', *β*'₁) and electron capture ($\gamma, \delta_1, \delta_2, \kappa_1, \kappa_2$) processes in He⁺-NO collision at $E = 0.5$ keV, as a function of τ . In order to clarify the presentation of the data, several charge-exchange channels which display similar τ and E dependence have been summed for the following energy-loss slices: κ_1 , $3 < Q < 10$ eV; κ_2 , $10 < Q < 18$ eV; κ_3 , $Q > 18$ eV. γ stands for the sum of the γ_i charge-exchange channels probabilities.

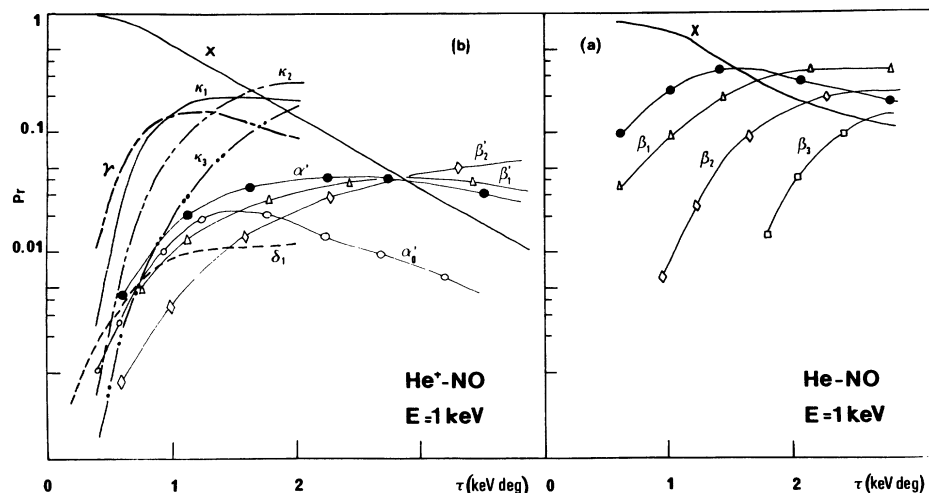


FIG. 10. (a) Relative probabilities P_i of electronic excitation of NO by He impact at $E = 1$ keV, as a function of τ . X refers to elastic scattering and $\alpha, \beta_1, \beta_2, \beta_3$ refer to electronic states of CO. [See text and Table II(a).] (b) Relative probabilities P_i for direct excitation ($\alpha', \beta'_1, \beta'_2$) and electron capture ($\gamma, \delta_1, \delta_2, \kappa_1, \kappa_2, \kappa_3$) processes in He⁺-NO collisions at $E = 1$ keV. $\gamma, \kappa_1, \kappa_2, \kappa_3$ are defined in Fig. 9(b).

$P_\alpha(\tau)$ probability reaches its maximum around $\tau = 1.5$ keV deg at $E = 1$ keV, whereas the $P_{\beta_i}(\tau)$ curves associated with the higher excited Rydberg series increase with increasing τ and then become constant at $\tau \cong 2.5$ keV deg. This behavior is very similar to the He-CO collision [Figs. 2(a) and 3(a)].

B. He⁺-NO collisions

1. Energy-loss spectra: direct excitation

At small reduced scattering angles ($\tau < 1$ keV deg) the ELS (Fig. 11) show that the lowest $A^2\Sigma^+$ and/or $a^4\Pi$ excited states of the target¹⁸ ($Q \cong 6$ eV) are prominently excited in contrast with the neutral He-NO system. When τ increases, the relative intensity of this 6-eV peak decreases and the excitation of the Rydberg series converging to the NO⁺(X) limit favors the 8-eV energy-loss structure ($E^2\Sigma^+, \dots$), similar to the He-NO collision. The 13–14-eV energy-loss structure, ascribed to the first states of Rydberg series¹⁹ converging to the $a^3\Sigma^+$ limit dominates the $Q > 11$ eV energy-loss range up to $\tau \cong 2$ keV deg. For the largest values of the explored τ range, the He⁺-NO ELS display similar trends to those observed for the He-NO collision (Sec. IV A 1).

2. Energy-loss spectra: electron-capture processes

For the lowest values of τ , several peaks show up in the vicinity of the $Q = 0$ eV energy loss ($-3 < Q < 3$ eV) and dominate the ELS (Fig. 12). Among these structures, two peaks can be unambiguously identified using the compilation of the NO⁺ states.²⁰ The δ_1 peak ($Q \cong -1.2$ eV) corresponds to the highest excited state of NO⁺ known spectroscopically [$\Delta E \cong 23.2$ eV above the NO(X) origin, repulsive $B^1\Pi$ or $B'^1\Sigma^+$ (Ref. 20)]. The δ_2 peak ($Q = -3$ eV) reflects the excitation of the $C^3\Pi$ or $B^1\Pi$ NO⁺ state²⁰ which has its well centered at $r_e = r_{e,NO(X)}$; in agreement with the FC prediction the NO⁺ ($C, v = 0$) level is prominently populated which gives rise to an especially narrow peak in the ELS. Besides these structures, other resolved peaks are observed at $Q \cong 0$ eV (γ_1), $Q \cong 0.6$ eV (γ_2), and $Q = 1.6$ eV (γ_3) (± 0.2 eV). The energy position of these NO⁺ states in the FC region is $\Delta E \cong 24.6, 25.1$, and 26.2 eV (± 0.2 eV), respectively.

For increasing values of τ , excitation of the endothermic channels dominates the excitation of exothermic channels.

a. *Exothermic channels.* Apart from the previously mentioned $B^1\Pi$ ($Q \cong -1.2$ eV) and $C^3\Pi$ ($Q \cong -3$ eV) NO⁺ states, the ELS show the population of the following charge-exchange channels:

$$\left. \begin{array}{l} \delta_3, \quad -7 \leq Q \leq -5.5 \text{ eV}, \quad Q_{\max} \cong -6 \text{ eV}, \quad \text{NO}^+(A^1\Pi, w^1\Delta) \\ \delta_4, \quad Q \cong -8 \text{ eV}, \quad \text{NO}^+(b^3\Pi, a^3\Sigma^+) \\ \delta_5, \quad Q \cong -15 \text{ eV}, \quad \text{NO}^+(X) \text{ very weak} \end{array} \right\} + \text{He}(1s^2).$$

As a general feature of the He⁺-diatom systems which we have explored, the relative intensity of exothermic channels δ_i decreases with increasing energy defect of the reaction.

b. *Endothermic channels.* The observation of three groups of partially resolved structures $\kappa_1, \kappa_2, \kappa_3$ can be ascribed to the series (in eV)

$$\text{He}(1snl) + \text{NO}^+(X) \quad (\kappa_1), \quad \text{with } 4.8 \leq Q \leq 9.6$$

$$\text{He}(1snl) + \text{NO}^+(a^3\Sigma^+ \rightarrow A^1\Pi) \quad (\kappa_2), \quad \text{with } 11.5 \leq Q \leq 16.2 \rightarrow 19.2$$

$$\text{He}(1snl) + \text{NO}^+(C^3\Pi, B^1\Pi) \quad (\kappa_3), \quad \text{with } Q \geq 18.$$

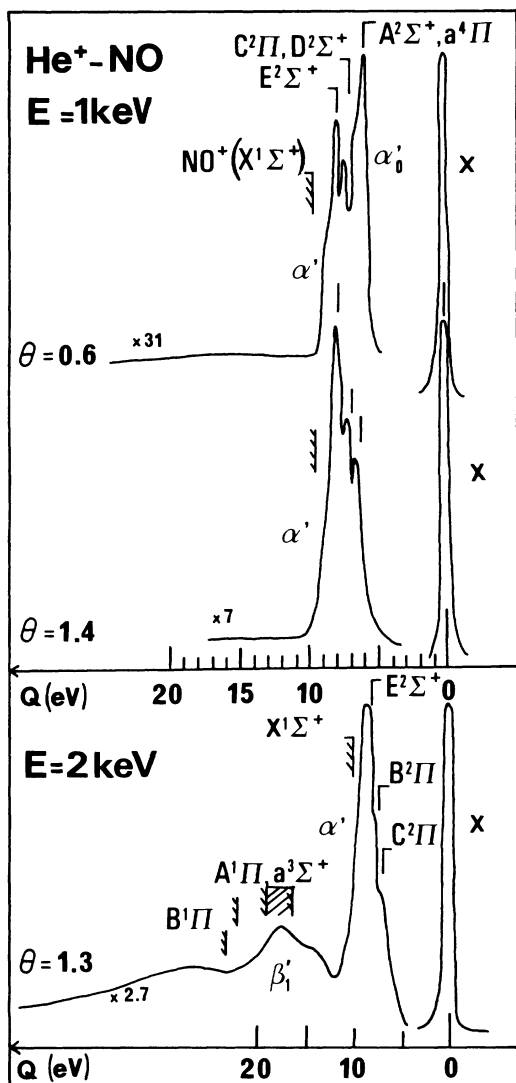
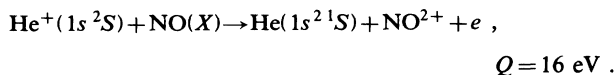


FIG. 11. ELS of scattered He^+ from $\text{He}^+\text{-NO}$ collision as a function of scattering angle θ . [See text and Table II(b) for identification.]

There is a strong indication that electron-capture processes lead to excited He products with or without simultaneous excitation of the ionized target. For $Q > 16$ eV these structures are superimposed on a tail which corresponds to the transfer ionization channel



The overlap of the κ_1 series with the $\text{He}(1s^2) + \text{NO}^{2+}$ series renders the detailed identification of the peaks rather intricate. Nevertheless, two additional peaks ϕ_1 ($Q \cong 3.5$ eV) and ϕ_2 ($Q \cong 10$ eV) are ascribed to excitation of NO^{2+} states, the energy positions of which in the FC region are $\Delta E \cong 28.1$ and 34.5 eV (± 0.2 eV), respectively.

c. Identification of the $\gamma_1, \gamma_2, \gamma_3, \phi_1, \phi_2$ peaks. The states corresponding to $\gamma_1, \gamma_2, \gamma_3, \phi_1, \phi_2$ peaks (Fig. 12)

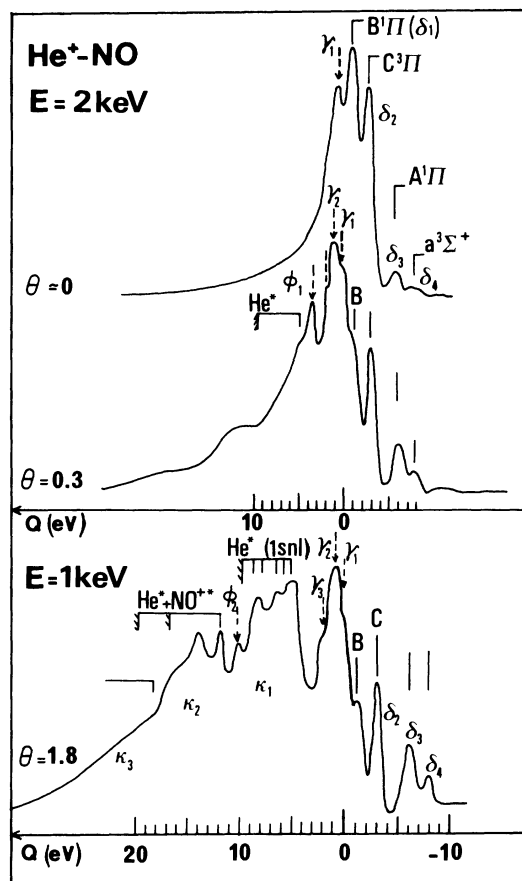


FIG. 12. ELS of scattered He from $\text{He}^+\text{-NO}$ collisions as a function of scattering angle. [See text and Table II(b) for identification.] Dashed arrows correspond to new states of NO^+ , the identification of which is discussed in the text.

could not be identified using the data in the literature. No well-resolved peaks were observed by photoelectron or photoionization spectroscopy, although some authors²¹ report that significant intensity is present in the 25–35-eV energy range. Similar arguments as those involved for the $\text{He}^+\text{-CO}$ case (Sec. III B 2) enable us to assign the γ_i and ϕ_i peaks to NO^{2+} states which differ by two electrons from the NO ground-state configuration. Indeed, Lefebvre *et al.*²² have shown that in the 24-eV region the $(4\sigma)^{-1} \text{NO}^+$ valence states are perturbed by NO^{2+} states coming from the $(5\sigma)(1\pi)^3(2\pi)^2$ configuration. More generally, the rearrangement of two electrons of the three outermost 5σ , 1π , and 2π molecular orbitals gives rise to five ionic series that can be labeled as $[(5\sigma)^2(1\pi)^4(2\pi)]^{-2}(n\lambda)$. The lowest state of each series is given in Table III. Since no calculation exists for such NO^+ states one can tentatively estimate their energy position by using the Koopman theorem if the energy positions of the corresponding neutral configuration states are known. The results displayed in Table III show that this rough estimation is consistent with the energy position of the $\gamma_1, \gamma_2, \phi_2$ peaks measured in the present data. Consequently, we tentatively attribute the γ_i and ϕ_i peaks to excitation of $[(5\sigma)^2(1\pi)^4]^{-2}(2\pi)^2$ states of NO^+ .

TABLE III. Estimation of the energy positions of NO⁺⁺ (5σ)(1π)³(2π)² and (5σ)²(1π)²(2π)² states using the Koopman theorem and the calculated energies of the NO* (5σ)²(1π)³(2π)² valence states given in Refs. 22, 23, and 24.

Lowest NO ⁺ state	Corresponding neutral state	ΔE _{FC} (neutral) (eV)	ΔE _{FC} (ion) (eV)
(5σ) ² (1π) ³ (6σ) (5σ)(1π) ⁴ (6σ)	(5σ) ² (1π) ⁴ (6σ)A ² Σ ⁺	6	22.2
			22.6
(5σ) ² (1π) ² (2π) ²	(5σ) ² (1π) ³ (2π) ²	7.2	23.4, 26.1, 35eV
			9.9
(5σ)(1π) ³ (2π) ²	P ² Π	18.8	23.8, 26.5, 35.4
(5σ) ⁰ (1π) ⁴ (2π) ²	(5σ)(1π) ⁴ (2π) ²		

3. Relative probabilities of the collision processes

The relative probabilities of direct and charge-exchange processes have been determined in the same way as in the He⁺-CO case [Figs. 9(b) and 10(b)]. Similar salient features are observed.

(i) The electron capture is the major process in the explored E, τ range and, in particular, the quasisonant charge-exchange channels are dominant for the lowest τ values.

(ii) The excitation probabilities of the near-resonant charge-exchange channels ($\gamma_i, \delta_1, \delta_2$) reach a maximum around $\tau=0.8$ keV deg. Their relative importance decreases with increasing energy.

(iii) The excitation of endothermic charge-exchange channels κ_i strongly increases with increasing τ and E .

(iv) The relative probabilities of direct excitation channels reach a flat maximum around $\tau \cong 1.5$ keV deg and increase, but weakly, with increasing energy.

These results compared with the measurements of the relative abundance of NO⁺, N⁺, and O⁺ ions produced by electron capture in the He⁺-NO collision ($I_{N^+} \gg I_{NO^+} > I_{O^+}$) establish that the NO⁺⁺ states populated by near-resonant charge exchange (γ_i) are dissociative or predissociative.

V. DISCUSSION

Owing to the similarities between the He⁽⁺⁾-CO and -NO collisions and the He⁽⁺⁾-N₂, -O₂, and -H₂ results, the discussion deals with the three main mechanisms responsible for inelastic processes in these systems. These mechanisms are indicated schematically on the qualitative state diagram (Fig. 13) extrapolated from the He⁺-N₂ and -O₂ examples. The processes are direct charge exchange into the exothermic channels, electronic transition favored at MO crossings and two-electron jumps due to the initial He 1s vacancy, and will be discussed successively in Secs. VA–VC below.

A. Charge exchange into the exothermic channels

The electronic configurations of the exothermic channels He(1s²) + BC⁺⁺ (valence) on Fig. 13 (Tables I and II) are generated by one-electron transition from the

valence orbitals of the diatom to the He 1s orbital. The general features, which have been observed are (i) the population of exothermic channels decreases strongly with increasing energy defect of the reaction, (ii) the very weak excitation of the lowest exothermic channels ($|Q| \geq 4$ eV) compared to the excitation of the endothermic channels with the same energy defect, (iii) the strong increase with increasing energy of the exothermic channel populations, and (iv) their appearance for the smallest τ values. These features are all characteristic of a direct transition of the Demkov-Nikitin type.²⁵ Accordingly, we can estimate the charge-exchange probability between the entrance channel and the exothermic channel i using the formula

$$P_{\delta_i} = \frac{1}{2} \operatorname{sech}^2 \frac{\pi}{v\sqrt{2}} \frac{\Delta\epsilon_i}{\sqrt{I_0 + \sqrt{I_i}}}, \quad (2)$$

where I_0 and I_i are the binding energies of the electron in

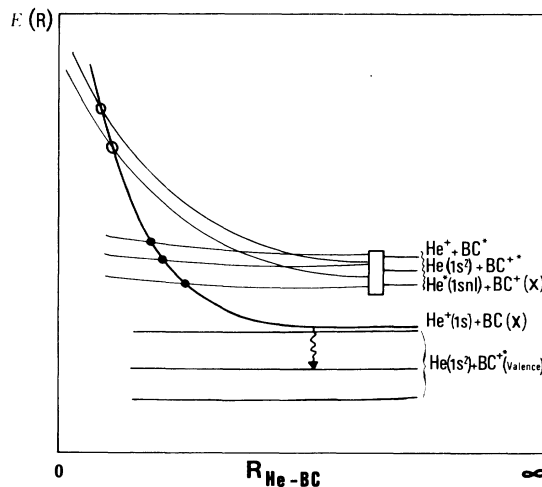


FIG. 13. Schematic qualitative state correlation diagram for the He⁺-BC system; the three main collision primary mechanisms are symbolized. Wavy arrow, direct Demkov-Nikitin-type transition between the entrance channel and exothermic charge-exchange channels. Solid circle, curve crossing where a two correlated electron transition (diabatic-II mechanism) takes place. Open circle, curve crossing associated with an MO curve crossing subsequent to MO promotion. At this crossing one- or two-electron jumps are favored. Open rectangle, secondary mechanisms which share the population due to primary excitation among outgoing channels which energetically overlap.

the initial and final states, $\Delta\epsilon_i$ is the corresponding resonance energy defect, and v is the collision velocity.

Although the calculated excitation probabilities [Eq. (2)] of the channels that are closest to resonance are too large by a factor of 5–10 with respect to experiment, such deviations can be understood for the following reasons. The two-state approximation may not be justified as there are many final states. Furthermore, the anisotropy of the relevant interactions, due to the relative orientation of the diatom and the collision axes, is not taken into account.

We now consider exothermic charge-exchange channels characterized by large energy defects from resonance ($\delta_2, \delta_3, \delta_4$, Figs. 5 and 12). In order to avoid systematic errors inherent in the measurement of total electron-capture probabilities at small angles the ratio of the δ_i peaks to δ_1 have been directly measured on the ELS and compared with the calculated ratios [Eq. (2)] for the various channels. In these cases, the Demkov-Nikitin mechanism is found to underestimate the charge-exchange probability by orders of magnitude.

To account for the population of such channels we propose the following two-step mechanism: (i) a Demkov-type charge-exchange transition populates the closest exothermic channels and (ii) once populated, these channels act as “relays” to populate those which lie a few eV below; such direct one-electron transitions between two levels separated by few eV are known to exist for atom-atom collisions in this velocity range.²⁶

B. Transitions between MO's

In contrast with the direct transition mechanism discussed in Sec. V A, electronic transitions may occur at MO curve crossings as suggested by the electron promotion model (Fig. 13). We proceed in this section to the investigation of such transitions.

From the data of Secs. III and IV it is seen that the neutral and ionic systems display great similarities for $\tau \geq 2$ keV deg, namely, the following.

(i) The same excited states of the target are preferentially populated by He and He^+ impact. For example, the dominant excitation of CO^* series associated with the $\text{CO}^{+*}(1\pi)^{-1} A^2\Pi$ and $\text{CO}^{+*}(1\pi)^{-2} D^2\Pi$ cores suggests that the $1\pi_{\text{CO}}$ orbital is promoted in both neutral and ionic cases. Similarly, the direct NO excitation ELS show the active roles played by the $1\pi_{\text{NO}}$ and $5\sigma_{\text{NO}}$ electrons in both He-NO and He^+ -NO collisions.

(ii) The relative excitation probabilities display similar trends. The probabilities for one-electron excitation processes reach a flat maximum around $\tau=1.5$ keV deg whereas those associated with doubly excited states keep on increasing with increasing τ until they reach a plateau.

Owing to the complexity of the $\text{He}^{(+)}\text{-CO}$ and -NO systems we do not attempt to build detailed triatomic correlation diagrams.² Nevertheless, the main features of the diabatic correlation diagrams obtained by making a cut at $r=r_e$ of the MO surfaces can be tentatively guessed, extrapolating the knowledge accumulated for atom-atom collisions.

In this schematic diagram (Fig. 14), we consider only the outer occupied orbitals of the projectile (He 1s) and the target ($1\pi_{\text{BC}}, 5\sigma_{\text{BC}}$) since the inner electrons do not partici-

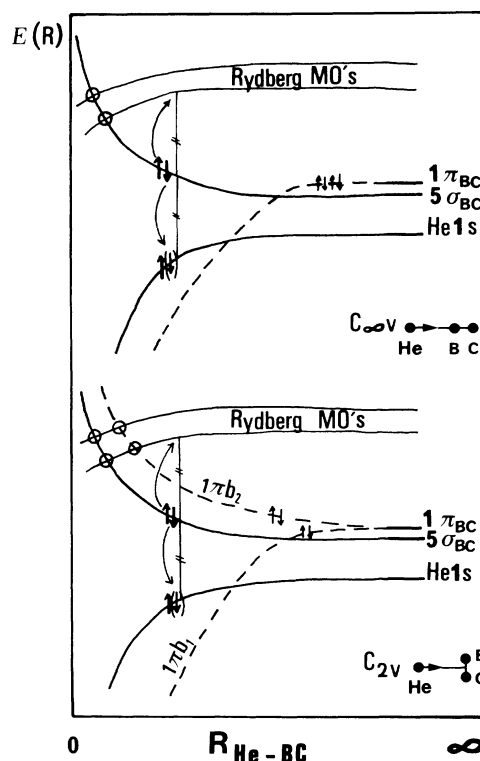


FIG. 14. Schematic MO correlation diagram for the $\text{He}^{(+)}\text{-BC}$ system in $C_{\infty v}$ and C_{2v} symmetries of the triatomic molecule. For both neutral and ionic systems MO promotion gives rise to MO crossings at which one- or two-electron jumps are favored. For the $\text{He}^+\text{-BC}$ case, the He 1s vacancy is responsible for the occurrence of two correlated electron transitions as illustrated by the two arrows on the diagram.

pate to the collision. When the two partners approach each other, the exchange interaction between the $1s_{\text{He}}$ and the σ_{BC} outer MO's is responsible for their mutual repulsion and induces the promotion of the σ_{BC} MO which is located above the $1s_{\text{He}}$ orbital as $R \rightarrow \infty$. The crossings undergone by the promoted and filled MO with initially empty MO's favor the excitation of one and/or two electrons of the target (diabatic-I mechanism).

Considering the 5σ and 1π MO's which lie close to one another the correlation diagram leads to different predictions according to the particular symmetry point group of the $\text{He}^{(+)}\text{-BC}$ triatomic molecule.

In the $C_{\infty v}$ symmetry (linear conformation) the doubly degenerate 1π MO is correlated with the united atomlike $2p\pi$ inner orbital; consequently, the 1π electrons are not expected to be excited during the collision, whereas the 5σ MO should be promoted.

On the other hand, in the C_{2v} symmetry (isosceles triangle) the $1\pi_{b_1}$ MO is similarly correlated to the united atomlike $2p\pi$ orbital whereas the $1\pi_{b_2}$ MO undergoes a promotion comparable to that of the 5σ MO in $C_{\infty v}$.

This primary DI mechanism is responsible for the direct single and double excitation of the target which was observed for both neutral and ionic systems in the large τ range. For the $\text{He}^+\text{-CO}$ (-NO) ionic systems, these one- and two-electron direct excitation channels turn out to en-

energetically overlap the He* (1snl)+BC⁺(X) and He⁺+BC⁺⁺ series, respectively, and a secondary mechanism involving one- or two-electron transitions is expected to mediate the population of the observed direct and exchange channels. The outgoing channels populated via a common DI primary mechanism should accordingly display similar τ dependences: This is actually the case for the χ_i and K_i charge-exchange probabilities which exhibit the same dependence as the β_i direct excitation probabilities [Figs. 3(b) and 10(b)].

C. Two-electron jumps due to the initial He 1s vacancy: diabatic-II process

The efficiency of the correlated two-electron transitions (diabatic-II process) related to the existence of the 1s_{He} inner vacancy in He⁺-diatom collisions has been established previously.² Such a mechanism involves the simultaneous jump of two electrons from an outer occupied orbital: One electron fills the He 1s vacancy and the other jumps to an empty higher-lying MO (Fig. 14), conserving energy in the process. This diabatic-II mechanism should populate the He(1s²)+BC⁺⁺ Rydberg series, where the BC⁺⁺ electronic configuration differs by two electrons from the BC ground state.

A strong indication for the efficiency of the DII process in He⁺-CO (-NO) collisions is provided by the large excitation of the γ , ϵ , η (γ_i, ϕ_i) charge-exchange channels in the low τ range ($\tau \leq 1$ keV deg) especially at low energy (see Secs. III B and IV B). It is noticeable that in this energy and angular regime the processes characterizing DI processes are much weaker as demonstrated by the comparison of the He⁺-CO (-NO) and the He-CO (-NO) data. Since the He(1s²)+CO⁺⁺ (NO⁺⁺), He* (1snl)+CO⁺(X) [NO⁺(X)], and He⁺+CO* (NO*) Rydberg series overlap (Fig. 13) a secondary mechanism is expected to share the primary DII excitation among these channels.

VI. CONCLUSION

At the end of this series of papers it may be worth recalling that most of the work to date using, for example,

optical and ion fragment measurements gave only a very limited insight into the general mechanisms governing the ion (atom)-molecule collisions. On the contrary, ELS measurements, even with a limited energy resolution, provide an overall view of the excitation mechanisms, their relative importance, and the evolution of their probabilities as a function of angle and energy. We think that this was a necessary step for understanding the basic collision mechanisms in ion (atom)-molecule collisions, in the medium energy range. The present investigation of He⁽⁺⁾-CO and -NO collisions confirms the qualitative understanding gained from the previously studied He⁽⁺⁾-diatom systems. Staying on a qualitative basis, it is noteworthy that these mechanisms are the same as in He⁽⁺⁾-rare-gas collisions, namely, the following.

(i) Direct Demkov-type transitions populate the exothermic charge-exchange channels and produce diatomic ions in valence states. These states may then act as relays to populate other exothermic channels which lie far from resonance.

(ii) MO promotion is a common feature to all neutral and ionic systems, and gives rise to electronic transitions at the related MO crossings (DI mechanism).

(iii) Specific to He⁺-target collisions, correlated two-electron transitions (DII mechanism) lead to direct excitation and charge-exchange processes.

An interesting outcome of the DII mechanism is that it creates molecular ions which are seldom dominantly excited by more conventional spectroscopy. This collision spectroscopic tool could be extended to investigate more complex molecular ions provided that a more accurate TOF spectroscopy be achieved. Specific to ion (atom)-molecule collisions, the role played by the relative orientation of the interparticle axes must be studied.

ACKNOWLEDGMENTS

We thank Dr. V. Sidis for enlightening discussions during the course of the work. Acknowledgments are due to Professor D. Pritchard for his suggestions to improve the presentation of the manuscript.

¹D. Doweck, D. Dhucq, J. Pommier, Vu Ngoc Tuan, V. Sidis, and M. Barat, Phys. Rev. A **24**, 2445 (1981).

²D. Doweck, D. Dhucq, V. Sidis, and M. Barat, Phys. Rev. A **26**, 746 (1982).

³J. C. Brenot, D. Dhucq, J. P. Gauyacq, J. Pommier, V. Sidis, M. Barat, and E. Pollack, Phys. Rev. A **11**, 1245 (1975).

⁴T. F. Moran and R. J. Conrads, J. Chem. Phys. **58**, 3793 (1973).

⁵E. Gustafsson and E. Lindholm, Ark. Fys. **18**, 219 (1960).

⁶(a) J. E. Parker and R. Y. Haddad, Int. J. Mass Spectrom. Ion Phys. **27**, 403 (1978); (b) R. Browning, C. J. Latimer, and H. B. Gilbody, J. Phys. B **2**, 534 (1969).

⁷J. E. Parker, and R. Y. Haddad, Int. J. Mass Spectrom. Ion Phys. **31**, 103 (1979).

⁸J. C. Brenot, J. Pommier, D. Dhucq, and M. Barat, J. Phys. B **8**, 448 (1975).

⁹S. G. Tilford and J. D. Simmons, J. Phys. Chem. Ref. Data **1**, 164 (1972).

¹⁰(a) N. Padial, G. Csanak, B. V. McKoy, and P. W. Langhoff,

J. Chem. Phys. **69**, 2992 (1978); (b) E. Lindholm, Ark. Fys. **40**, 103 (1969).

¹¹M. Okuda and N. Jonathan, J. Electron Spectrosc. Relat. Phenom. **3**, 19 (1974).

¹²G. H. Bearman and J. J. Leventhal, Phys. Rev. A **17**, 80 (1978).

¹³R. Loch, Chem. Phys. **22**, 13 (1977).

¹⁴K. Codling and A. W. Potts, J. Phys. B **7**, 163 (1974).

¹⁵(a) J. L. Gardner and J. A. R. Samson, J. Chem. Phys. **62**, 1447 (1975); (b) L. Åsbrink, C. Fridh, E. Lindholm, and K. Codling, Phys. Scr. **10**, 183 (1974); (c) A. Hamnett, W. Stoll, and C. E. Brion, J. Electron Spectrosc. Relat. Phenom. **8**, 367 (1976).

¹⁶(a) G. R. Wight, M. J. Van der Wiel, and C. E. Brion, J. Phys. B **9**, 675 (1976); (b) H. Oertel, H. Schenk, and H. Baumgärtel, Chem. Phys. **46**, 251 (1980); (c) L. C. Lee, R. W. Carlson, D. L. Judge, and M. Ogawa, J. Chem. Phys. **63**, 398 (1975).

¹⁷M. A. Coplan and K. W. Ogilvie, J. Chem. Phys. **61**, 2010 (1974).

- ¹⁸F. R. Gilmore, *J. Quant. Spectrosc. Radiat. Transfer* **5**, 369 (1965).
- ¹⁹(a) O. Edqvist, E. Lindholm, L. E. Selin, H. Sjögren, and L. Åsbrink, *Ark. Fys.* **40**, 439 (1969); (b) K. P. Huber, *Helv. Phys. Acta* **34**, 929 (1961); (c) R. M. Reese and H. M. Rosenstock, *J. Chem. Phys.* **44**, 2007 (1966).
- ²⁰D. L. Albritton and A. L. Schmeltekopf, *J. Chem. Phys.* **71**, 3271 (1979).
- ²¹(a) C. E. Brion and K. H. Tan, *J. Electron Spectrosc. Relat. Phenom.* **23**, 1 (1981); (b) K. Siegbahn *et al.*, *ESCA applied to Free Molecules* (North-Holland, Amsterdam, 1969).
- ²²H. Lefebvre-Brion, *Chem. Phys. Lett.* **9**, 463 (1971).
- ²³H. Lefebvre-Brion and C. M. Moser, *J. Chem. Phys.* **44**, 2951 (1966).
- ²⁴R. Gallusser and K. Dressler, *J. Chem. Phys.* **76**, 4311 (1982).
- ²⁵Y. N. Demkov, *Zh. Eksp. Teor. Fiz.* **45**, 195 (1963) [*Sov. Phys.—JETP* **18**, 138 (1964)]; E. E. Nikitin, *Advances in Quantum Chemistry* (Academic, New York, 1970), Vol. 5.
- ²⁶N. Andersen, in *Proceedings of the Eleventh International Conference on the Physics of Electronic and Atomic Collisions, Kyoto, 1979*, edited by K. Takayanagi and N. Oda (The Society for Atomic Collisional Research, Kyoto, 1979), p. 301.